AGU PUBLICATIONS

JGR

Journal of Geophysical Research: Atmospheres

RESEARCH ARTICLE
10.1002/2017JD027515

Key Points:
- A methodology has been developed for VIIRS-based CrIS cloud clearing for CrIS radiance assimilation in cloudy skies
- Quality control steps on VIIRS-based CrIS cloud-cleared radiances (CCRs) are important for applications due to lack of absorption bands in VIIRS
- The impacts on the forecast fields of Hurricanes Joaquin (2015) and Matthew (2016) show potential operational application of VIIRS-based CrIS CCRs in NWP

Correspondence to:
J. Li,
jun.li@ssec.wisc.edu

Citation:
Wang, P., Li, J., Li, Z., Lim, A. H. N., Li, J., Schmit, T. J., & Goldberg, M. D. (2017). The impact of Cross-track Infrared Sounder (CrIS) cloud-cleared radiances on Hurricane Joaquin (2015) and Matthew (2016) forecasts. *Journal of Geophysical Research: Atmospheres*, *122*. https://doi.org/10.1002/2017JD027515

Received 26 JUL 2017
Accepted 30 NOV 2017
Accepted article online 7 DEC 2017

©2017. American Geophysical Union. All Rights Reserved.

The Impact of Cross-track Infrared Sounder (CrIS) Cloud-Cleared Radiances on Hurricane Joaquin (2015) and Matthew (2016) Forecasts

Pei Wang[1], Jun Li[1], Zhenglong Li[1], Agnes H. N. Lim[1], Jinlong Li[1], Timothy J. Schmit[2], and Mitchell D. Goldberg[3]

[1]Cooperative Institute for Meteorological Satellite Studies, University of Wisconsin-Madison, Madison, WI, USA, [2]Center for Satellite Applications and Research, NESDIS, NOAA, Madison, WI, USA, [3]NOAA JPSS Program Office, Lanham, MD, USA

Abstract Hyperspectral infrared (IR) sounders provide high vertical resolution atmospheric sounding information that can improve the forecast skill in numerical weather prediction. Commonly, only clear radiances are assimilated, because IR sounder observations are highly affected by clouds. A cloud-clearing (CC) technique, which removes the cloud effects from an IR cloudy field of view (FOV) and derives the cloud-cleared radiances (CCRs) or clear-sky equivalent radiances, can be an alternative yet effective way to take advantage of the thermodynamic information from cloudy skies in data assimilation. This study develops a Visible Infrared Imaging Radiometer Suite (VIIRS)-based CC method for deriving Cross-track Infrared Sounder (CrIS) CCRs under partially cloudy conditions. Due to the lack of absorption bands on VIIRS, two important quality control steps are implemented in the CC process. Validation using VIIRS clear radiances indicates that the CC method can effectively obtain the CrIS CCRs for FOVs with partial cloud cover. To compare the impacts from assimilation of CrIS original radiances and CCRs, three experiments are carried out on two storm cases, Hurricane Joaquin (2015) and Hurricane Matthew (2016), using Gridpoint Statistical Interpolation assimilation system and Weather Research and Forecasting-Advanced Research Version models. At the analysis time, more CrIS observations are assimilated when using CrIS CCRs than with CrIS original radiances. Comparing temperature, specific humidity, and U/V winds with radiosondes indicates that the data impacts are growing larger with longer time forecasts (beyond 72 h forecast). Hurricane track forecasts also show improvements from the assimilation of CrIS CCRs due to better weather system forecasts. The impacts of CCRs on intensity are basically neutral with mixed positive and negative results.

1. Introduction

Satellite sounder observations, such as those from microwave and infrared (IR) sounders, have shown large impacts on numerical weather prediction (NWP) in operations and research studies (Cardinali, 2009; Kelly & Thepaut, 2007; Le Marshall et al., 2005, 2006). Hyperspectral IR sounders, such as the Infrared Atmospheric Sounder Interferometer and the Atmospheric Infrared Sounder (AIRS) (Cucurull et al., 2014; Joo et al., 2013), can provide high vertical resolution of atmospheric temperature and moisture information. The assimilation of hyperspectral IR sounders has a large impact on global NWP models (Garand et al., 2013; Smith et al., 2015).

The Cross-track Infrared Sounder (CrIS) is NOAA's new generation hyperspectral IR sounder onboard Suomi-NPP launched on 28 October 2011 (experimental) and on the upcoming Joint Polar Satellite System (JPSS) series (operational). CrIS has 1,305 IR sounding channels covering wavelengths from 3.92 μm to 15.38 μm (655–2550 cm^{-1}). The spatial footprint is 14 km at nadir with a scanning swath of 2,200 km. Due to the relatively large spatial footprint, a CrIS FOV (field of view) has relative low possibility to be completely clear. Most IR sounder data assimilation is limited to clear skies or clear channels that are not affected by clouds, which reduces the application of these high-quality observations in high impact weather (HIW) forecast, such as tropical cyclone (TC) and local severe storm forecasts. Therefore, how to handle clouds and increase the usage of information in cloudy skies for IR sounder assimilation is an important research topic (Bauer et al., 2011; Geer & Bauer, 2011; Li et al., 2016; Pangaud et al., 2009; Pavelin et al., 2008; Wang et al., 2014).

A cloud-clearing (CC) technique, which removes the cloud effects from a partially cloud-filled IR FOV and derives the cloud-cleared radiances (CCRs) or clear-sky equivalent radiances, is an alternative way to

assimilate thermal dynamical information from IR sounders in cloudy skies. Removing the effects of clouds from a partially cloud-filled FOV requires additional or supporting information. Depending on the type of supporting information needed, three types of CC methodologies have been developed: (a) imager-based CC: using collocated high-resolution imager IR radiances and cloud information (Li et al., 2005); (2) microwave-based CC: using collocated microwave sounder radiances for removing cloud effects (Susskind et al., 2006); and (3) background-based CC: using NWP background information for deriving CCRs (Liu, Collard, & Derber, 2015). Both imager-based and microwave-based CCRs are background independent. Imager-based CCRs maintain a single IR FOV basis for assimilation, while background-based and microwave-based IR CCRs degrade the resolution to that of a microwave footprint—for example, from 13.5 km to 45 km at nadir for AIRS CCRs. The imager-based CC method has been successfully applied to AIRS CCRs. The assimilation of AIRS CCRs improved the analyses temperature fields and hurricane track forecasts (Wang et al., 2015).

The imager-based CC method uses the high spatial resolution observations from an imager, especially one with an IR sounder onboard the same platform, to provide accurate high-resolution cloud mask information. Similar to the AIRS and Moderate Resolution Imaging Spectroradiometer (MODIS) cloud-clearing method (Li et al., 2005), Visible Infrared Imaging Radiometer Suite (VIIRS) provides the high-resolution imager data onboard Suomi-NPP, which provides high-quality cloud mask information for CrIS CCRs. However, due to differences between the AIRS/MODIS and CrIS/VIIRS (Visible Infrared Imaging Radiometer Suite) observing systems, special attention is needed to apply the imager-based CCR technique to CrIS/VIIRS: (1) adapting the MODIS/AIRS cloud-clearing algorithm to VIIRS/CrIS by taking into account the geometry differences between the MODIS/AIRS and VIIRS/CrIS observing systems; (2) adding quality control (QC) steps as needed to account for spectral differences: MODIS has nine absorption bands including four CO_2 absorption bands in the longwave IR spectral region, two CO_2 absorption bands in the shortwave IR spectral region, two water vapor absorption bands, and one ozone absorption band in the 9.6 μm region; in contrast, VIIRS does not have any absorption bands in the IR spectral region, which could increase the uncertainties of CrIS CCRs in absorption spectral regions (Li et al., 2014); (3) validating CrIS CCRs and the impact of CrIS CCRs on NWP are important for broader applications.

In this paper, the description of the CrIS CC methodology is discussed in section 2. Section 3 introduces the data, models, and experimental design. Section 4 analyzes the data impacts and the differences in the atmospheric fields at the analysis time. The forecast fields and the atmospheric structure are further discussed in section 5. The summary and future works are given in section 6.

2. CrIS Cloud-Clearing Methodology

CrIS is a hyperspectral infrared sounder onboard the Suomi National Polar-orbiting Partnership (Suomi NPP) and future JPSS satellites with 1,305 channels from 3.92 μm to 15.38 μm. VIIRS provides high-resolution imager data onboard the same platform as CrIS. VIIRS has 22 spectral bands from 0.412 μm to 12.01 μm with 16 moderate resolution (750 m) channels and 6 imaging resolution channels (Lee et al., 2006). VIIRS provides high spatial resolution observations of clouds and the Earth's surface, including a cloud mask (Hutchison et al., 2005), cloud particles (Godin, 2014; Pavolonis & Heidinger, 2004), cloud top parameters (Baker, 2012), cloud optical thickness, and effective radius (Godin, 2014). With the collocation technique developed by Nagle (Nagle, 1998; Nagle & Holz, 2009), the high spatial resolution VIIRS cloud mask can be used to detect clouds within CrIS FOVs. For each CrIS FOV, only if 95% of the FOV coverage is clear based on the collocated VIIRS cloud mask, this CrIS FOV is identified to be purely clear. The radiances from these CrIS FOVs along with the radiances from CrIS clear channels are assimilated in operational NWP systems. Li et al. (2016) showed that the assimilation of clear CrIS FOVs with the VIIRS cloud mask can reduce the hurricane track root-mean-square-error (RMSE) compared to the assimilation of clear CrIS FOVs with stand-alone cloud detection in the 72 h forecasts. The results are consistent with MODIS clear detection for AIRS radiance assimilation (Li et al., 2004; Wang et al., 2014). Applying the imager cloud information in data assimilation effectively reduces the cloud contaminated IR radiances, and improves the analysis and forecast atmospheric fields (Eresmaa, 2014).

Assimilating only clear FOVs or clear channels results in rejecting all the cloud-affected CrIS radiance observations, which could contain critical information about a weather system, especially in cloudy region. One effective way to utilize those cloud-affected radiance observations is to extract the radiances from the clear portion of partially cloudy FOVs, or so-called cloud clearing (Smith et al., 2004). The cloudy information from

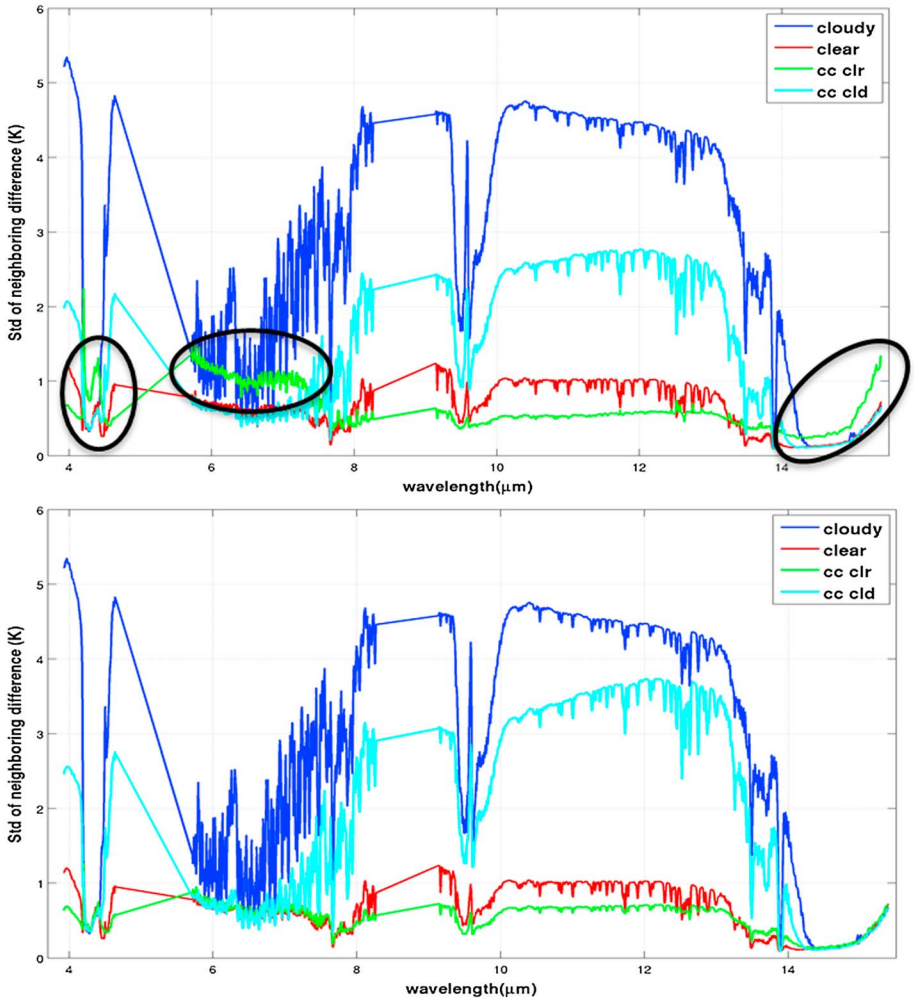

Figure 1. The standard deviation of the neighboring differences for three classes of CrIS FOVSs (top) before and (bottom) after the two quality control steps: cloudy (overcast, blue), clear (red), and partially cloudy before (cyan) and after (green) the cloud clearing. The black ellipses highlight the unrealistic standard deviation after the cloud clearing for high peaking channels. They are fixed after the two quality control steps applied.

VIIRS provides the information necessary to remove the cloud impacts from CrIS cloudy radiances. For cloud-clearing CrIS FOVs, the following assumptions are required: the atmospheric state is homogenous in two adjacent CrIS FOVs, and the cloudiness is uniform with the same cloud optical depths and cloud top height, while the differences are in cloud emissivity and fractional cloud coverage. More details on the algorithm can be found in Li et al. (2005).

Due to the lack of absorption bands on the VIIRS (only three surface channels are available for use), some of the CrIS CCRs are found to have low quality in the high peaking channels (CO_2 and H_2O absorption bands). In order to eliminate those CrIS CCRs, two additional quality control (QC) steps are implemented. The first QC is the similarity test, which is to abandon pairs of similar FOVs from CC. The CC technique requires the pair of neighboring FOVs to be substantially different (otherwise, the pair will have the same information, not enough for CC). Any N* (the ratio of cloud effective coverage of two FOVs) between 0.25 and 4 (N* of 1 indicates two identical FOVs) are considered similar, and no CC will be performed. The second QC step is the homogeneous test, which removes pairs of FOVs that break the assumption of a homogeneous atmosphere. For example, cloudy radiances are usually colder than clear. Therefore, for a pair of neighboring FOVs, the one with more cloud cover should be colder. If that is not the case, no CC will be performed for that pair of CrIS FOVs. After the two additional QC steps, the remaining CrIS CCRs can be assimilated as clear radiances in the data assimilation system without changes of observational error covariance and assimilated channels. The

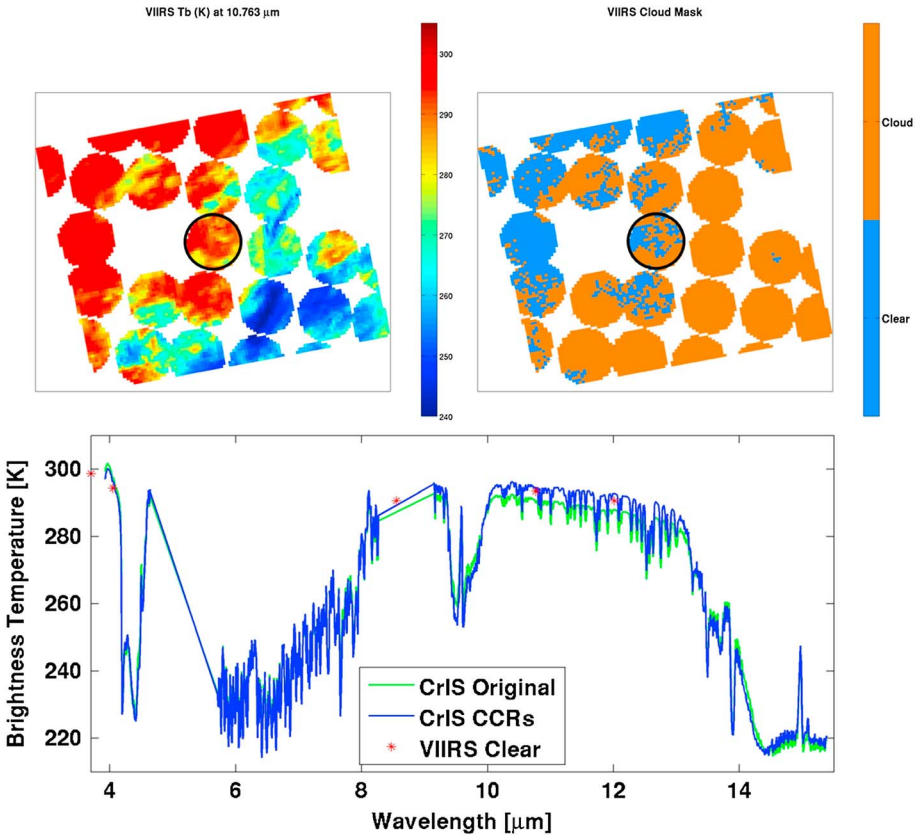

Figure 2. (top left) VIIRS brightness temperature image using band M15 (wavelength 10.763 μm) (unit: K). (top right) Cloud mask from VIIRS at the same time. (bottom) The BT of the original CrIS (green line) and CCRs (blue line) at the same location (see the black circle in Figure 2), as well as mean clear VIIRS BTs (red star) (unit: K).

advantages of this CC imager-based method are that it maintains the original footprint of the CrIS data and no background information is needed. It is important to point out that the AIRS/MODIS CC does not suffer from the difficulties discussed above because there are multiple CO_2/H_2O absorption bands from MODIS, which allow a thorough evaluation of AIRS CCR using MODIS radiances. Any pairs of FOVs breaking the similarity and homogeneous tests will unlikely pass the radiance evaluation.

Figure 1 shows the standard deviation (SD) of the neighboring differences for three classes of CrIS FOVs: cloudy (overcast), clear, and partially cloudy before and after the cloud clearing. These values tell the spatial homogeneousness for each class. As shown in Figure 1 (top), the SD of partially cloudy neighboring differences before cloud clearing is in between the cloudy and clear. A successful cloud clearing should bring that spectrum closer to the clear spectrum, which is true for most of low channels. As a matter of fact, those channels have even smaller SDs than the clear spectrum after the cloud clearing. This is reasonable because the cloud-clearing technique uses neighboring information, which smoothens out the spatial gradient to some extent. However, the high peaking channels (around 4.3, 5.8–6.5, and 15 μm), highlighted by the black ellipses, have increased SDs after the cloud clearing, even larger than those from cloudy FOVs, which is clearly unrealistic. Especially those channels peaking in stratosphere (around 4.3 and 15 μm) are not affected by clouds at all. They should have similar SDs as cloudy and clear classes. This indicates that some CrIS FOVs are cloud cleared with low quality. After applying the two quality control steps, the CrIS FOVs violating the similarity and the homogeneous tests are abandoned, and the results in Figure 1 (bottom) are more reasonable for those high peaking channels.

The following parts provide a demonstration of the CC method and its application. The CrIS cloud mask is derived from the VIIRS cloud mask product (IICMO). VIIRS BT (brightness temperature) image using band M15 with a central wavelength of 10.763 μm is shown in Figure 2 (top left). It appears that the selected

CrIS FOV is partially covered by clouds (colder brightness temperature or brighter color) in the green circle. This is confirmed by the high spatial resolution VIIRS cloud mask in Figure 2 (top right). Figure 2 (bottom) shows the CrIS CCRs BT spectrum for all 1,305 channels (blue line) along with the original CrIS BT spectrum (green line) at the same location in the black circle of Figure 2 (top). It can be seen that the CrIS CCRs BTs are warmer than the original CrIS BTs especially at the window channels, indicating that CC is able to reduce the cloud impacts. The red star denotes the mean clear-sky VIIRS BT within this CrIS FOV, which can be used as a reference for CrIS CCR. The good agreement between CrIS CCRs and VIIRS clear observations indicates that the VIIRS-based CrIS CC technique is effective to reduce the cloud impact and produce radiances as if the skies were clear. Validation with the neighboring clear CrIS radiances also indicates that CrIS CCRs after QC have reasonable accuracy and precision (Haixia LIU, personal communication).

The optimal cloud-clearing method (Li et al., 2005) is applied to CrIS data to calculate the CrIS CCRs. Although for the experimental domain and the time period (details in section 3) only 14% of the partially cloudy CrIS FOVs are successfully cloud-cleared, these additional "clear equivalent" radiances will make a substantial improved impact on the analysis and forecast, as will be shown in sections 4 and 5.

3. Hurricanes, Models, and Experimental Design

3.1. Hurricane Joaquin (2015)

Hurricane Joaquin was a destructive, powerful, and long-lasting tropical cyclone in the Atlantic Ocean in 2015. It started on 27 September 2015 and rapidly intensified as it moved southwest to the Bahamas. Because of its unique track, Joaquin was one of the tropical cyclones (TCs) that are most difficult to predict; it took a very sharp turn from its southwest movement to the northwest with a close approach to Bermuda on 2 October 2015. The spread among the track forecasts by different models caused large uncertainties in how Joaquin would affect the eastern United States. The majority of tracks from operational models forecasted that Joaquin would move close to or make landfall on the eastern United Sates. The operational 120 h forecasts from different models from 0600 UTC 29 on September to 1800 UTC on 1 October 2015 are shown in Figure 3. The best track is from NOAA's National Hurricane Center (NHC) (Berg, 2016). The NHC/Central Pacific Hurricane Center Forecast (OFCL) predicted that the track of Hurricane Joaquin would be close to the eastern United States; the HWRF track showed a landfall from 0600 UTC on 29 September to 0600 UTC on 1 October; the AVNO (Global Forecast System Model Forecast) and UKM (UKMET Model Forecast) tracks were correct and turned to the northeast at 0000 UTC on 1 October, while the UKM's hurricane track moved slower than the Best Track. Note that the track data from Best Estimate, HWRF, AVNO, and UKM are available at every 6 h for TC positions; the OFCL data are at every 0, 3, 12, 24, 36, 48, 72, 96, and 120 h forecasting time; the data from the UKM forecasting experiments are every 12 h.

3.2. Hurricane Matthew (2016)

Hurricane Matthew was a late-season, extremely strong, and long-lived tropical cyclone in the Atlantic Ocean in 2016. It was known as the costliest Atlantic hurricane since Hurricane Sandy (2012). It passed across Cuba and moved along the east coast of Florida and to the northeast. It first formed on 22 September as a tropical wave on the west coast of Africa and moved west. Early on 1 October, it weakened from Category 5 to a high-end Category 4. By late 1 October, it began to turn north and accelerate by 2 October. On 4 October it made landfall in Cuba and then it moved north thereafter. According to NHC, Matthew made landfall at South Carolina as a Category 1 hurricane. The storm caused an estimated 603 deaths, 1,657 injuries, and more than $15 billion (USD) in damages.

3.3. Developmental Testbed Center-Gridpoint Statistical Interpolation System

Gridpoint Statistical Interpolation (GSI) is a data assimilation system designed for both global and regional models (Kleist et al., 2009; Wu et al., 2002). It is primarily a three-dimensional incremental variational (3Dvar) system, and it has the option to be used as a hybrid data assimilation system as well (Wang et al., 2013). It was developed jointly by NOAA, NASA, and National Center for Atmospheric Research (NCAR) and used as an operational model in the National Centers for Environmental Prediction (NCEP) global model (Global Data Assimilation System (GDAS)), North American Mesoscale Forecast System (NAM), HWRF, Rapid Refresh (RAP), and other models. The Developmental Testbed Center (DTC) transitioned the operational GSI system into a community version for research study, real-time applications (i.e., Satellite Data

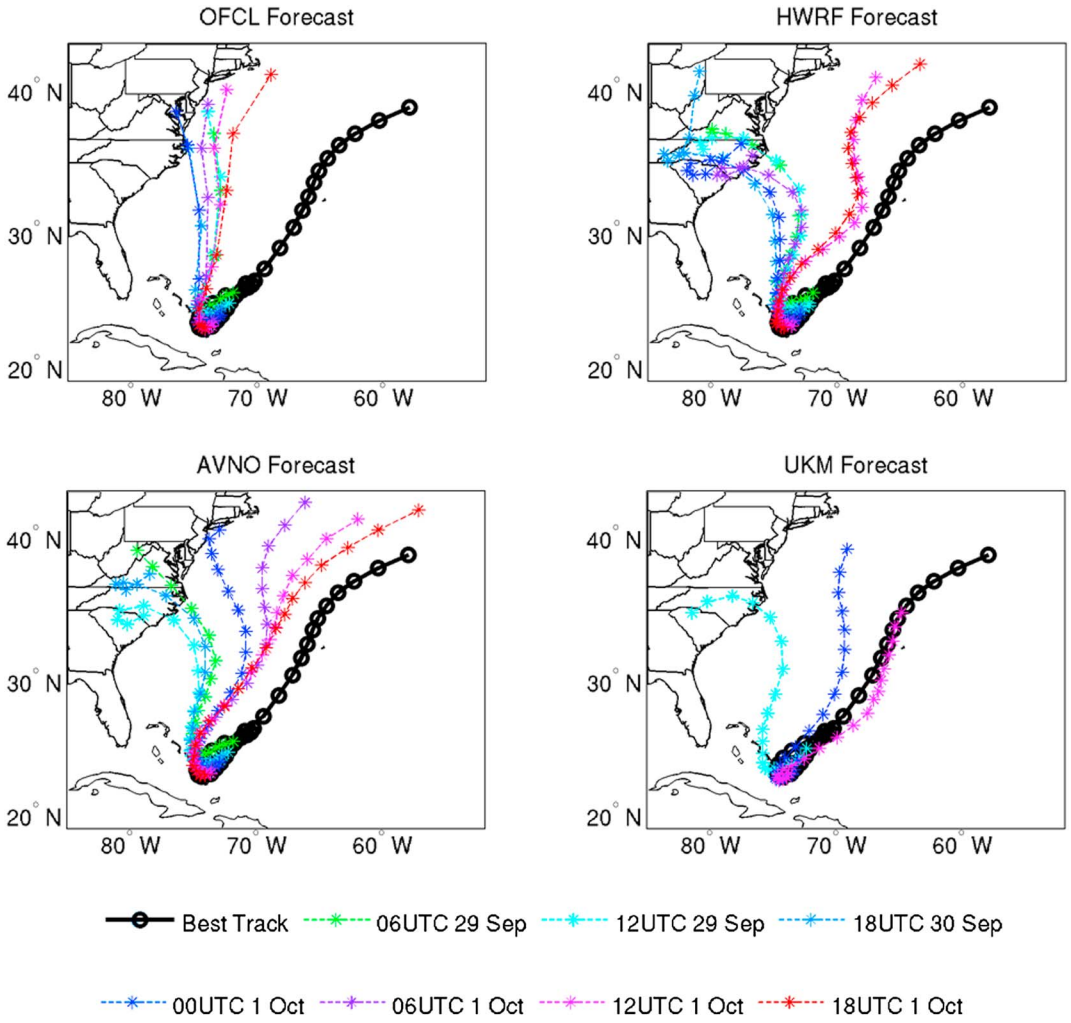

Figure 3. 120 h forecast track plots of the OFCL, HWRF model, AVNO, and UKM global model for the forecast cycles between 0600 UTC on 29 September and 1800 UTC on 1 October 2015 for Hurricane Joaquin. The best track of Joaquin is indicated by the black lines with six-hourly tropical cyclone positions. The dots for HWRF, AVNO, and UKM forecasts represent 6 h intervals, and OFCL represent 12 h intervals.

Assimilation for Tropical storm (SDAT): http://cimss.ssec.wisc.edu/sdat/), and case studies. Because GSI can assimilate many types of observations—conventional data, satellite radiances, radar data, etc.—it has been widely used in the research community (Lim et al., 2014; Han et al., 2016). DTC-GSI version 3.3 is used as the data assimilation system in this study. Due to the difficulty in generating the ensemble members for hybrid assimilation in regional models, the 3Dvar method is applied to assimilate the data and study the data impacts.

For satellite radiance assimilation, a forward radiative transfer model is required to simulate the radiance from the background. The community radiative transfer model (CRTM) is implemented in GSI for satellite radiance simulation and assimilation (Chen et al., 2010; Chen et al., 2012; Han et al., 2006). The coefficients of CRTM version 2.1.3 are used in this study.

3.4. Weather Research and Forecasting-Advanced Research Version Model

The advanced research version of the Weather Research and Forecasting (WRF-ARW) model is a community mesoscale model developed by the National Center for Atmospheric Research (NCAR). Since WRF-ARW was first released, it continues to be updated every year to implement additional physical schemes for research

Table 1
Experimental Design for CNTL, CrIS(org), and CrIS(CCRs)

Experiment	GTS	AMSU-A	ATMS	CrIS original	CrIS CCRs
CNTL	√	√	√		
CrIS(org)	√	√	√	√	
CrIS(CCRs)	√	√	√		√

and case studies. It is also used as an NWP model in operational centers and near-real-time systems, such as RAP and SDAT.

WRF-ARW version 3.6.1 is the NWP model used in this study. The horizontal domain covers 6°N to 51°N and 40°W to 100°W on the Lambert Conformal Conic projection. This region covers a large area of the North Atlantic Ocean, the East and Midwest of the United States, Cuba, the Gulf of Mexico, and the very northern part of South America. The horizontal resolution is 12 km with 400 * 350 grid points. The vertical resolution is 51 layers from the surface to 10 hPa instead of the default 50 hPa in the WRF model. The microphysics scheme is the WRF Single-Moment six-class scheme by Hong and Lim (2006), longwave and shortwave radiation schemes are the Rapid Radiative Transfer Model for General circulation model scheme (Iacono et al., 2008), the planetary boundary layer is the Yonsei University scheme (YSU) (Hong & Lim, 2006), and the cumulus parameterization is the Kain-Fritsch scheme (Kain, 2004).

3.5. Data and Experiments

The data assimilated in the experiments are as follows: Global Telecommunication System (GTS) represents the conventional data, including radiosondes, wind profilers, aircraft data, and surface observations; Advanced Microwave Sounding Unit (AMSU-A) radiances data are from NOAA 15, NOAA 18, NOAA 19, and Metop-A; Advanced Technology Microwave Sounder (ATMS) radiances data are from Suomi-NPP; CrIS original radiance data prepared from NOAA/NESDISE/STAR in Binary Universal Form for the Representation of meteorological data format; and CrIS CCRs radiances data are in the same format as CrIS original radiances, except that FOVs successfully cloud cleared are replaced with CrIS CCRs.

Three data assimilation experiments are carried out to study the impacts from the assimilation of original CrIS radiances and the assimilation of the CrIS CCRs in the regional model (Table 1).

1. GTS + AMSUA + ATMS or CNTL for simplicity
2. GTS + AMSUA + ATMS + CrIS or CrIS (org) for simplicity
3. GTS + AMSUA + ATMS + CrIS CCRs or CrIS (CCRs) for simplicity

All the experiments, CNTL, CrIS (org) (CrIS original radiances), and CrIS (CCRs), are conducted on Hurricane Joaquin (2015) from 0600 UTC on 30 September to 1800 UTC on 6 October 2015 (black line in Figure 4). The differences between CrIS (org) and CrIS (CCRs) are summarized below:

CrIS (org): clear FOVs in clear skies (GSI approach) + clear channels in cloudy skies (GSI approach) (McNally & Watts, 2003); CrIS (CCRs): clear FOVs in clear skies (VIIRS for detection), CCRs (VIIRS-based CC approach) in partial cloud cover.

For Hurricane Joaquin, the assimilation cycling runs every 6 h from 0600 UTC on 30 September to 1800 UTC on 1 October, and 120 h forecasts followed each assimilation step. Seven groups are carried out for the following discussions of the hurricane track and intensity forecasts.

For Hurricane Matthew, the assimilation is from 1800 UTC on 2 October to 1200 UTC on 4 October 2016. The assimilation runs every 6 h, followed by 120 h forecasts. The experimental designs and the model settings for the two hurricanes are the same. The forecast results of both hurricanes are shown in the following sections, while the discussions are focused on Hurricane Joaquin (2015).

The background fields at the initial time and the boundary conditions are from NCEP Final Operational Global Analysis data at every 6 h. The thinning mesh for CrIS radiances is every 60 km. The background error covariance, the observational error covariance, and the channel selections for satellite radiances are consistent with the NCEP operational system, i.e., NAM (McCarty et al., 2009). The variational bias correction method is used for the satellite bias correction (Zhu et al., 2014). Since the satellite radiances are assimilated in GDAS model at every analysis step, the global satellite bias coefficient, including CrIS, is used as the initial mass bias correction coefficient and angle bias coefficient for our assimilation although there is no spin-up period in the experiment. And then the bias correction coefficient is updated based on the previous results for each following cycling run.

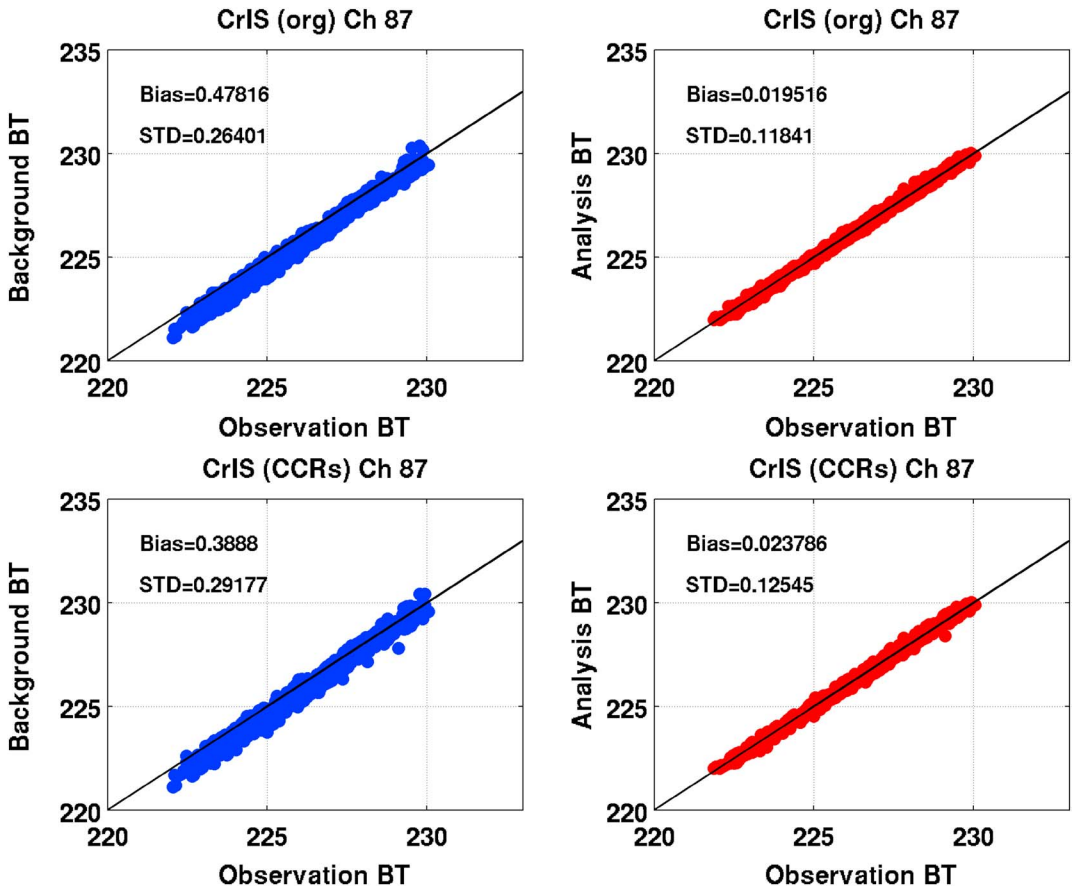

Figure 4. The scatterplots of the CrIS observed versus the simulated brightness temperatures (BTs) of channel 87 (unit: K). The BTs from the background are in blue dots, while the BTs from the analysis are in red dots. Both (top) CrIS (org) and (bottom) CrIS (CCRs) are shown.

4. Data Impacts at the Analysis Time

4.1. The Number of Assimilated Data

The temperature, moisture, and other atmospheric information from satellite observations can affect the background or first-guess fields through data assimilation. To better understand the data impacts from the different satellite observation data sets (i.e., CrIS (org) and CrIS (CCRs)), the assimilated data at the analysis time are discussed in this section.

Figure 4 shows the scatterplots of observed versus the simulated brightness temperatures (BTs) of CrIS channel 87 (703.75 cm^{-1}, with weighting function or radiance sensitivity function peaking at around 100 hPa) from the background (blue) and the analysis (red), respectively, for both CrIS (org) (Figure 4, top) and CrIS (CCRs) (Figure 4, bottom). The bias and standard deviation (SD) of O − A (observations minus analysis) are smaller than O − B (observations minus background) for both CrIS (org) and CrIS CCRs. The O − B of CrIS (CCRs) is slightly larger than O − B of CrIS (org), which might be due to the fact that CCRs are from cloudy skies and the observation error might be slightly larger than the clear radiances, while the O − A of the two experiments become closer to each other, which indicates that the CrIS CCRs are assimilated successfully in the experiments.

Figure 5 shows the CrIS radiance data used in GSI models after quality control at 0600 UTC on 30 September 2015 for Hurricane Joaquin. The data coverage of CrIS channel 87 (Figure 4, top) between CrIS (org) and CrIS (CCRs) shows that CrIS (CCRs) has more observations (408) assimilated than CrIS (org) (362 observations). For CrIS channel 130 (730.625 cm^{-1}, peaking at around 700 hPa) (Figure 4, bottom), there are 213 observations for CrIS (CCRs) and 166 observations assimilated for CrIS (org). Overall, there are 12.71% more observations

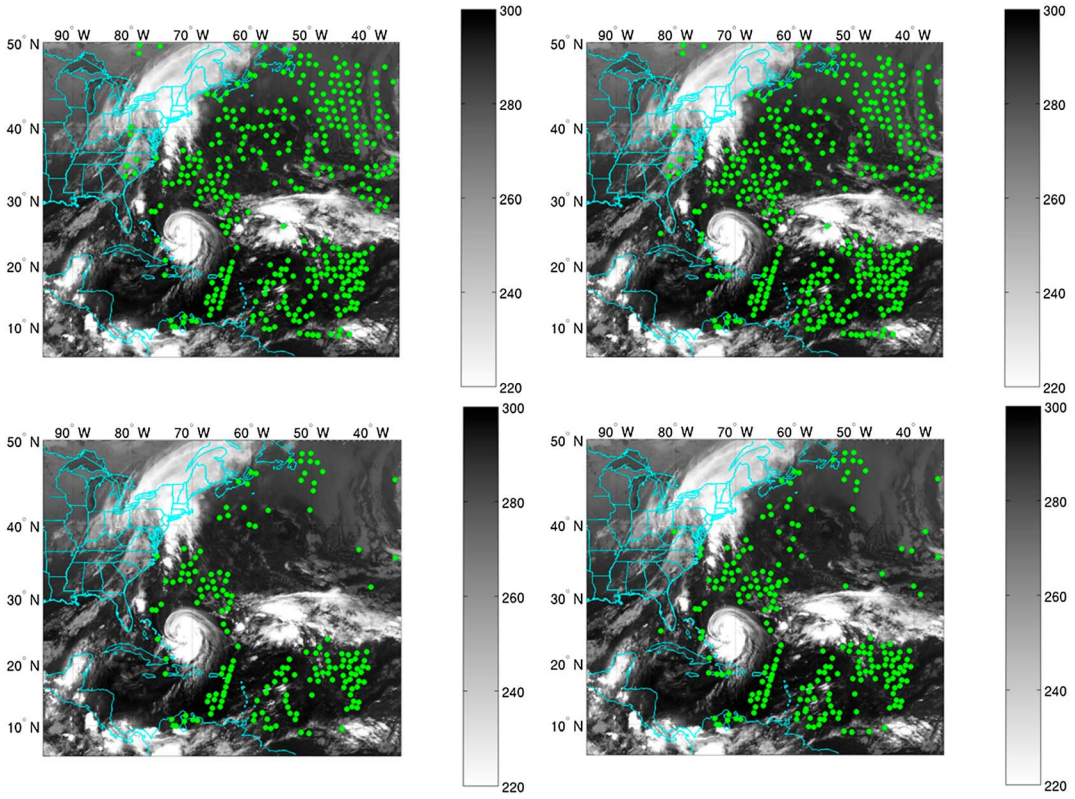

Figure 5. CrIS data coverage (green dots) for channel 87 from (top left) CrIS (org), (top right) CrIS (CCRs), for channel 130 of (bottom left) CrIS(org) and (bottom right) CrIS(CCRs) overlapped on GOES-15 Imager channel 11 μm (grey, unit: (K)) at 0600 UTC on 30 September 2015 for Hurricane Joaquin.

assimilated for channel 87, and 28.31% more observations for channel 130 at this analysis time. The total number of CrIS observations assimilated in GSI of CrIS (org) is 64405, and CrIS (CCRs) is 75,959 at 0600 UTC on 30 September 2015. Comparing the total number of assimilated CrIS radiances of these two experiments, there are around 17.9% more observations that are assimilated at this analysis time. For Hurricane Matthew, the total number of CrIS (org) is 50,976 and CrIS (CCRs) is 63,166 at 1800 UTC on 2 October 2016. There are around 23.9% more observations with the assimilation of CrIS CCRs data.

Based on the comparison of the number of assimilated CrIS radiances, CrIS CCRs data have different impacts for different channels. Since the weighting function peak of channel 87 is at around 100 hPa, while the peak of channel 130 is at around 750 hPa, channel 130 is more prone to clouds. For the higher peaking channels, the increase in assimilated CrIS data from CrIS (CCRs) is less dramatic because those channels are less likely affected by clouds (they are assimilated even when there are clouds). For lower peaking channels, the increase in assimilated CrIS data from CrIS (CCRs) is more significant. These additional observations assimilated will provide more useful information on the thermodynamic structures of the analysis atmospheric fields, especially in troposphere. Since the CC method focuses on obtaining clear equivalent radiances under partially cloudy regions, most successful CCRs are in the regions surrounding hurricanes. The observations near the hurricane core or under heavy thick clouds are still abandoned through the QC in the GSI model.

4.2. The Differences of Temperature Fields

The different data sets of CrIS (org) and CrIS (CCRs) directly affect the atmospheric fields at the analysis time. The differences in temperature fields between CrIS (org) and CrIS (CCRs) (CrIS (CCRs) minus CrIS (org)) at 0600 UTC on 30 September 2015 are shown in Figure 6. With CrIS CCRs, more observations are assimilated in the system, bringing in more temperature information from observations. The additional observations could affect the analysis fields, making them closer to the observations. From Figure 6, the regions showing temperature differences (shaded area) are consistent with the differences in data locations (Figure 5), which

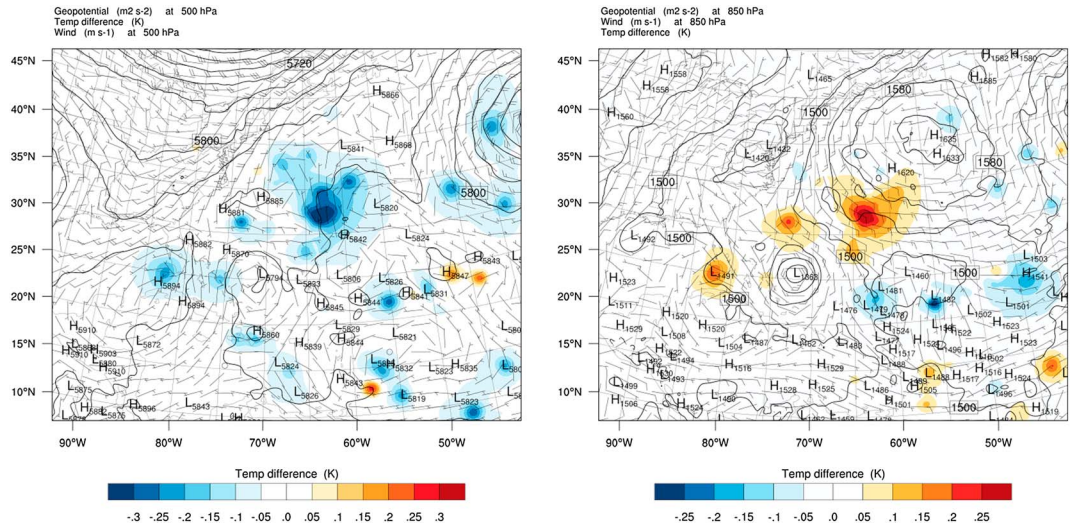

Figure 6. Temperature difference between CrIS(CCRs) and CrIS(org) (CrIS(CCRs) minus CrIS(org)) (shaded), geopotential heights of CrIS (contour), and wind vector of CrIS(CCRs) at (left) 500 hPa and (right) 850 hPa at 0600 UTC on 30 September 2015.

are the regions surrounding the hurricane center and the edge of clouds. In general, the analysis temperature is around 0.15 K colder from CrIS (CCRs) compared to CrIS (org), while the maximum cold temperature center is larger than 0.3 K. At 850 hPa, the analysis temperature fields are around 0.15 K warmer from CrIS (CCRs) than CrIS (org). Although the temperature differences are minimal at this analysis time, these differences could grow large enough to substantially affect the forecast. The temperature differences from the forecast will be discussed in the following sections.

5. Forecast Results

5.1. Temperature and Specific Humidity Forecast Fields

As noted earlier, the CrIS (CCRs) have more CrIS observations assimilated than the CrIS (org), which consequently affects the atmospheric analyses fields. The additional observations from CrIS (CCRs) adjust the temperature fields at the analysis fields and bring them closer to the observations. The slight temperature differences at the analysis time are amplified during the forecast time.

For Hurricane Joaquin, the standard deviation (SD) of temperature and specific humidity differences compared with conventional radiosonde for the 120 h forecast are shown in Figures 7a and 7b, respectively. Based on the pressure levels, the temperature SDs are divided into three layers, 1000–850 hPa, 850–400 hPa, and 400–100 hPa. The temperature SD of the CNTL is shown as the black line, the CrIS (org) in blue, and CrIS (CCRs) in red. The temperature SDs of the three group experiments are very close to each other for the first 48 h forecast. After that, differences start to emerge. At 72 to 96 h, the temperature of CrIS (CCRs) has larger temperature SD. For forecasts of 96 to 120 h, CrIS (CCRs) shows the smallest temperature SD for all three layers, which indicates that the forecast temperature fields of CrIS (CCRs) are the closest to the observations in the whole domain. Not surprisingly, the temperature SD of CNTL has the largest value at the 120 h forecast.

For specific humidity, similar results are shown in Figure 7b; CrIS (CCRs) has the smallest specific humidity SD for forecast of 96–120 h, and the CNTL has the largest SD. Differences become larger with longer forecast times. The temperature and specific humidity SD of the three group experiments are almost the same for the first 48 h. After 72 h, the differences in SD become larger. At 120 h, the CrIS (CCRs) gives the best forecasts of the temperature and moisture fields among the three experiments, and the CNTL has the worst forecast.

Figure 7c shows the SD of U wind differences compared to the dropwindsonde observations for the 120 h forecasts for Hurricane Joaquin (2015). The SD of V wind (figure not shown) differences has similar pattern

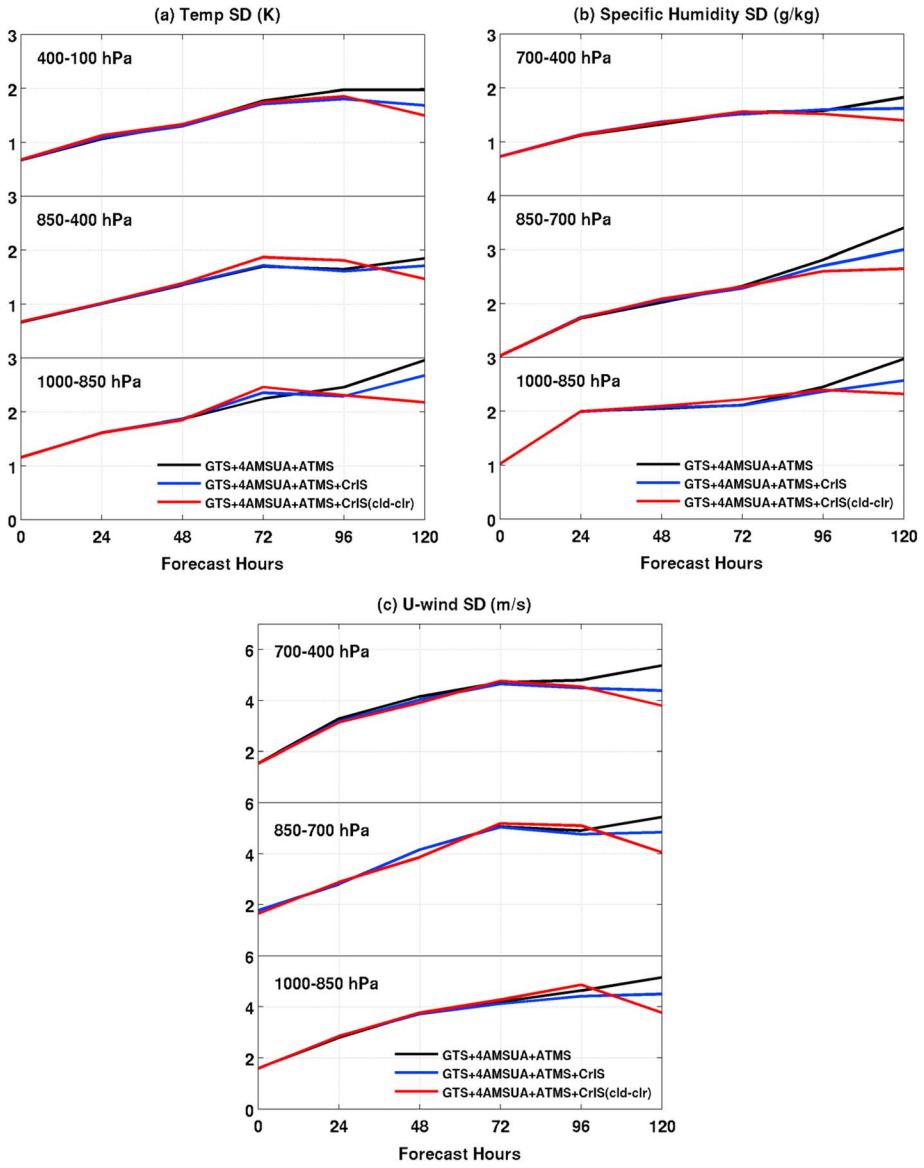

Figure 7. Temperature (a) SD, (b) specific humidity, and (c) U wind from radiosonde and CNTL (solid black), CrIS(org) (solid blue), and CrIS(CCRs) (solid red) during the 120 h forecast time for Hurricane Joaquin.

with U wind. The dropwindsonde is an ideal source to evaluate the environmental fields (Liu et al., 2012). The evaluation is also divided into three layers. For the first 48 h forecast, the SD of U and V wind is similar to the SD of temperature and specific humidity that the SD of three group experiments are very closed to each other. The differences of SD are becoming larger from 72 h to 120 h forecast. For U wind, the SD of 72 h and 96 h forecasts of CrIS (CCRs) is around 0.2 m/s larger than the other two experiments from 1,000 to 700 hPa. The SD of 120 h of CrIS (CCRs) is 1.3 m/s smaller than the other experiments for the whole three layers. The SD at 120 h for the three experiments are further discussed from 1,000 hPa to 200. At 120 h (Figure 8), the SD of CrIS (CCRs) shows consistence improvement from 1,000 hPa to 200 hPa with the value between 3.2 m/s and 5.6 m/s; the SD of CNTL is from 4.4 m/s to 7 m/s and SD of CrIS (org) is from 3.7 m/s to 5.9 m/s.

Based on the comparison of SDs, the assimilation of CrIS radiances may reduce the forecast error from the CNTL on temperature, moisture, and U and V wind fields in the troposphere after 72 h or 96 h, and the assimilation of CrIS CCRs may further reduce the forecast error and improve the temperature moisture and U and V forecasts.

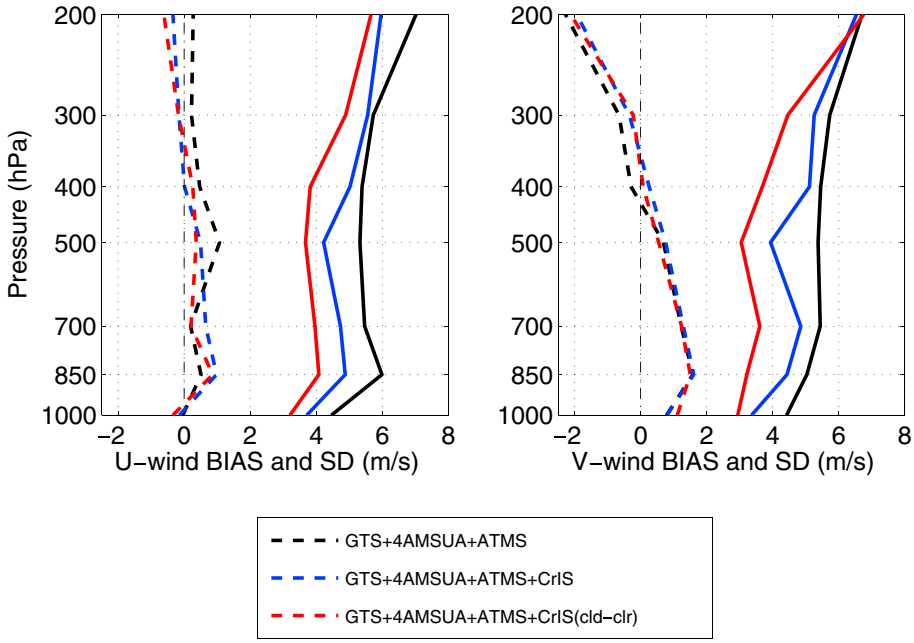

Figure 8. U and V wind BIAS (dashed lines) and SD (solid lines) from dropwindsonde and CNTL (black), CrIS(org) (blue), and CrIS(CCRs) (red, unit: m/s) at 120 h forecast time from 1000 to 200 hPa for Hurricane Joaquin.

5.2. Hurricane Track and Intensity Forecast Error

The 120 h forecast tracks of Hurricane Joaquin from the CNTL, CrIS (org), and CrIS (CCRs) are shown in Figure 9. The Best Track (black line) is from NHC's Hurricane Joaquin Report. At 0600 UTC and 1200 UTC on 30 September, all three forecast tracks of Joaquin turn west to the continent at some point, which is away from the Best Track. With the assimilation of CrIS (org) and CrIS (CCRs), the forecast tracks are closer to the Best Track. At 1800 UTC 30 on September and 0000 UTC on 1 October, the tracks of the CNTL and CrIS (org) still

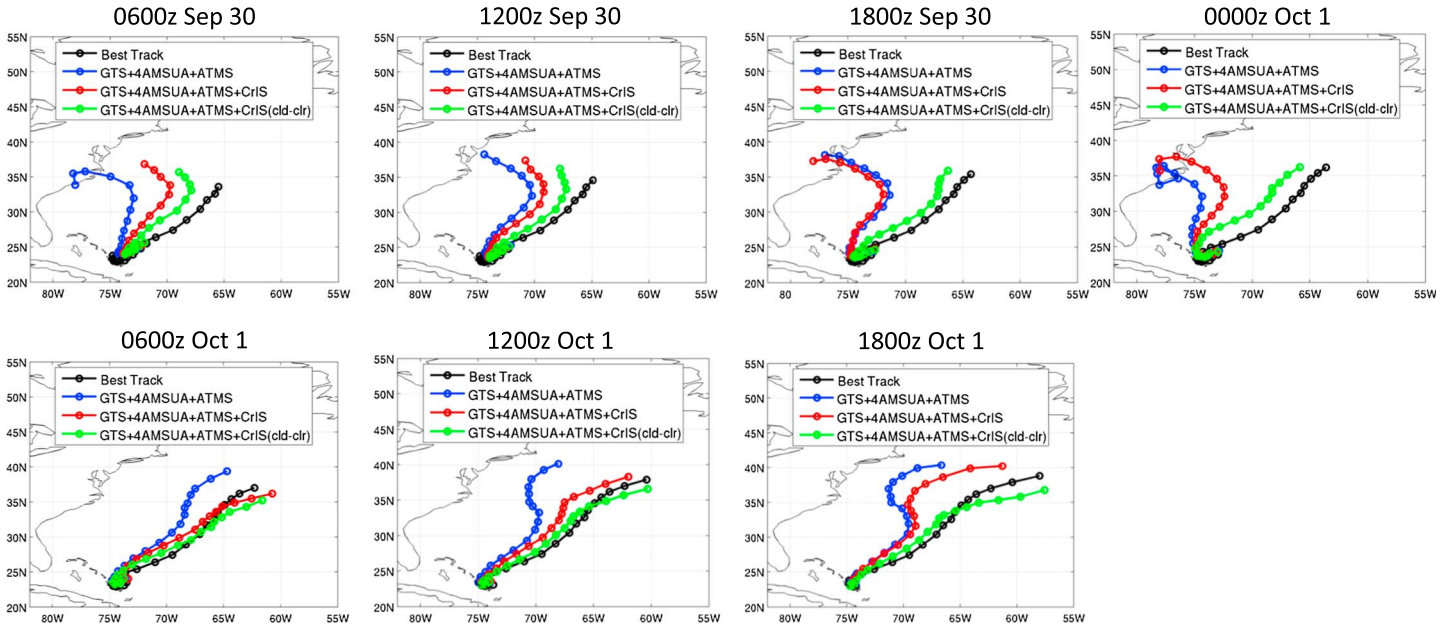

Figure 9. The 120 h track forecast from the Best Track (black), CTNL (blue), CrIS(org) (red), and CrIS (CCRs) (green) for Hurricane Joaquin from 0600 UTC on 30 September to 1800 UTC on 1 October.

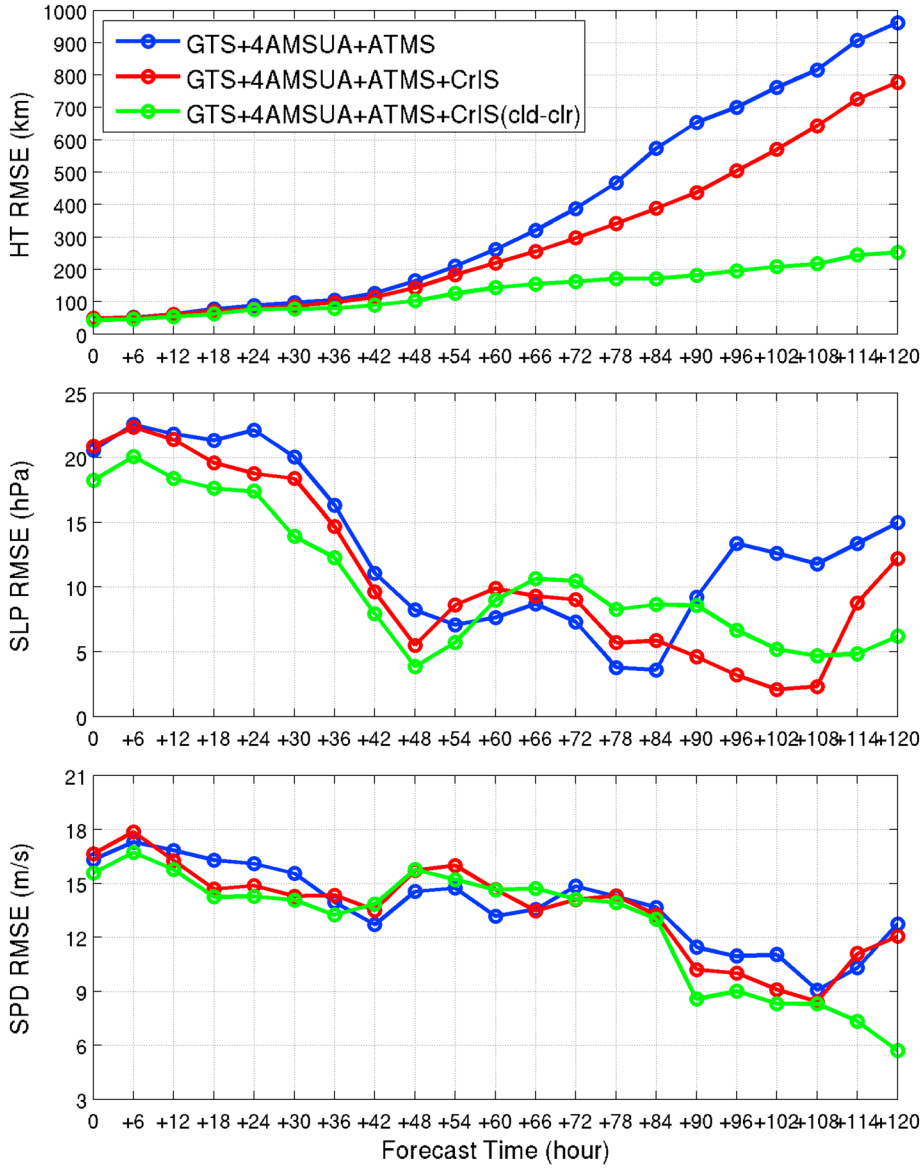

Figure 10. The (top) track, (middle) minimum sea level pressure, and (bottom) maximum wind speed forecast RMSE with CNTL (blue), CrIS (org) (red), and CrIS(CCRs) (green). Data are assimilated every 6 h from 0600 UTC on 30 September to 1800 UTC on 1 October 2015, followed by 120 h forecasts for Hurricane Joaquin.

turn to the west, but the CrIS (CCRs) forecast shows that the hurricane will move northeast, which is consistent with the Best Track. From 0600 UTC on 1 October, the three groups of experiments all forecast that the hurricane moves northeast. While the turning point of Hurricane Joaquin is hard to predict, the assimilation of CrIS (CCRs) is able to adjust the atmospheric fields based on the additional cloud-cleared observations and move the forecast track to the east from 1800 UTC on 30 September, which significantly reduces the track forecast error compared to the other experiments.

The root-mean-square-error (RMSE) of the hurricane track, minimum sea level pressure (SLP), and maximum wind speed (SPD) of the three experiments are shown in Figure 10 for Hurricane Joaquin. The minimum sea level pressure (SLP) and the maximum wind speed (SPD) are used to reflect the hurricane intensity forecast. The hurricane track and intensity forecast results are validated against the observations from the NHC report. The RMSE of the hurricane track of CrIS (CCRs) is the smallest among the three experiments during the 120 h forecasting. This is consistent with the track forecasts in Figure 9. The assimilation of CrIS (CCRs) significantly

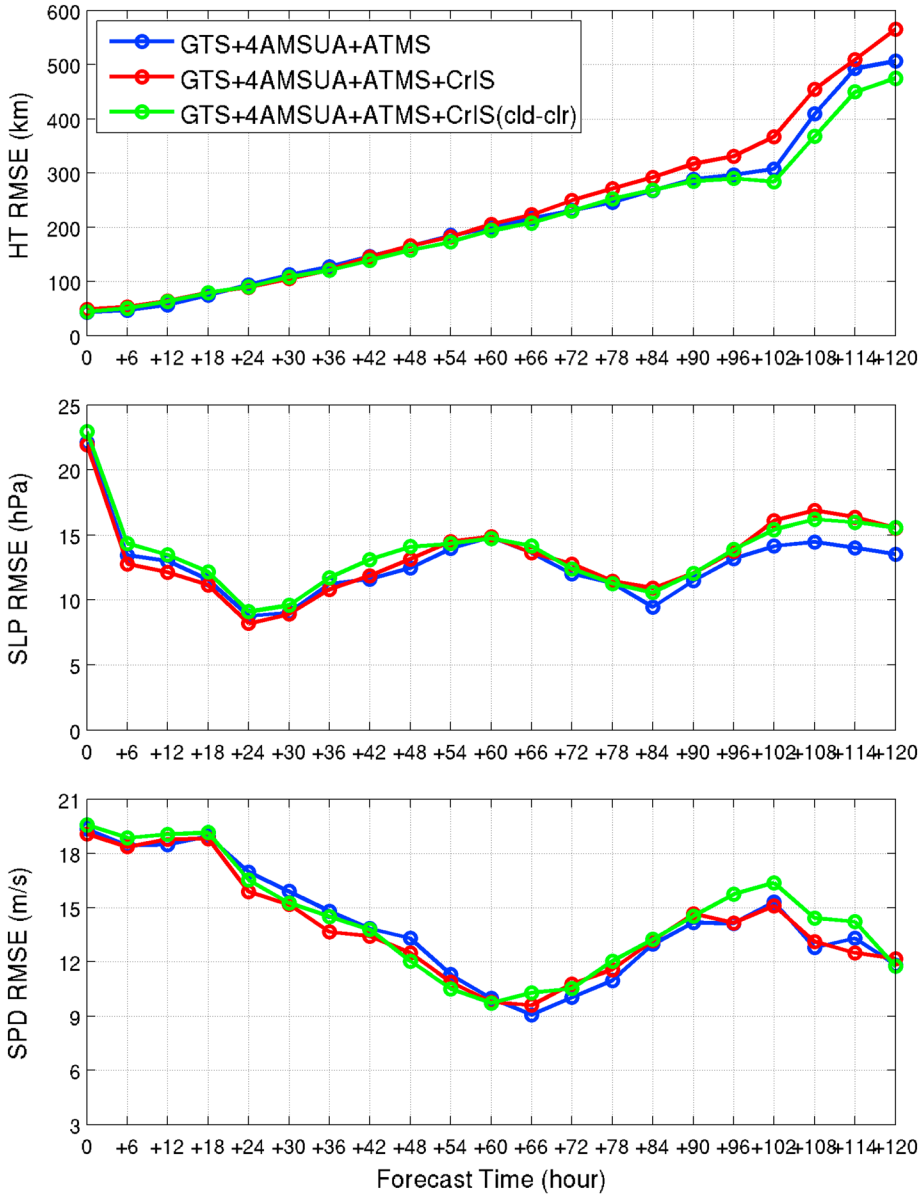

Figure 11. The same as Figure 13 but for Hurricane Matthew.

improves the track forecast of Hurricane Joaquin compared with that of CrIS (org), which also reduces the track RMSE compared with the CNTL run. For the hurricane minimum SLP and maximum SPD, the assimilation of CrIS (CCRs) shows only a neutral impact, although there is a visible decrease in SLP and SPD RMSE compared to the CNTL and CrIS (org) in the first 48 h.

The RMSE of the hurricane track, minimum SLP, and maximum SPD for Hurricane Matthew are shown in Figure 11. Compared with Hurricane Joaquin, the data impacts of CrIS radiances on the track forecast for Hurricane Matthew are much smaller. Since there is no sharp turning point for Hurricane Matthew, the track differences of the three experiments are relatively small. However, there is still a slight improvement in track forecasts with CrIS (CCRs). The track RMSE of CrIS (CCRs) is 11 km smaller than CrIS (org) for the 60 h forecast, and the difference in RMSE becomes larger with longer forecast times. At the 84 h forecast, the track RMSE of CrIS (CCRs) is around 23 km smaller, and at the 120 h forecast, the track RMSE of CrIS (CCRs) is more than 90 km smaller than CrIS (org). For the hurricane intensity, the RMSE of the three experiments are very

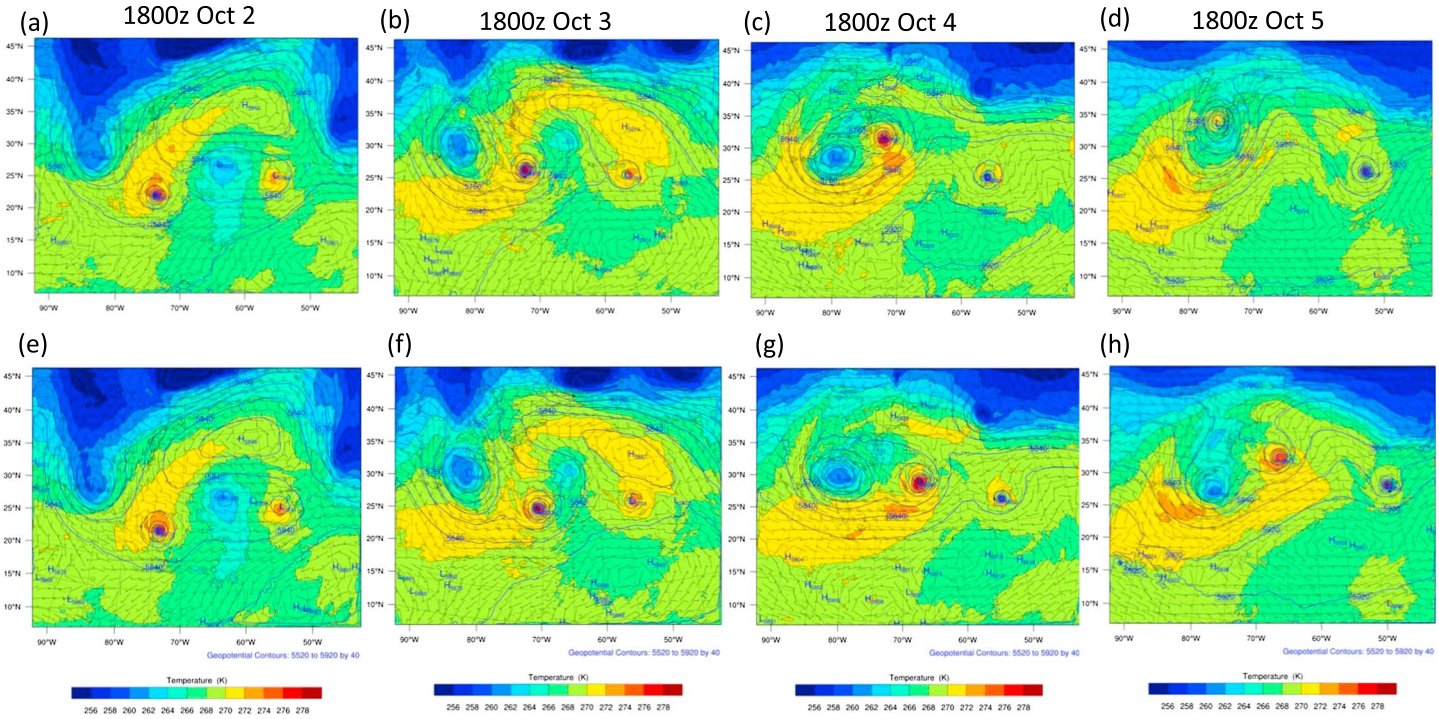

Figure 12. Temperature (shaded, unit: K), geopotential height (contour, unit: m^2/s^2), and wind vector (vector) at 500 hPa for 48 h, 72 h, 96 h, and 120 h forecasts from (a–d) CrIS (org) and (e–h) CrIS (CCRs) from 1800 UTC on 30 September 2015.

close. As with Hurricane Joaquin, the CrIS (CCRs) can improve the hurricane track forecasts, but the impacts are neutral for the intensity forecast.

5.3. The Impact Analysis on the 1800 UTC 30 September of Hurricane Joaquin (2015) Forecasts

Based on the forecast statistics for these two hurricanes, we found that the sharp turning point of Hurricane Joaquin is hard to predict, which also contributes to the smallest track RMSE of CrIS (CCRs) in the three experiments. The track forecast at 1800 UTC on 30 September 2015 gave the largest difference between CrIS (CCRs) and the other two experiments, CNTL and CrIS (org). The 120 h forecast atmospheric fields of CrIS (org) and CrIS (CCRs) are compared to further discuss the data impacts of the additional CrIS (CCRs) observations.

Hurricane Joaquin's center is in the western part of the Atlantic Ocean, and there is one strong cold low-pressure system over contiguous United States (CONUS) to the west of the hurricane's center. The intensity and the location of the low-pressure system could greatly affect the track of hurricane. The temperature, geopotential heights, and the wind structures are quite similar for the first 24 h forecasts (figures not shown) from both the CrIS (org) and CrIS (CCRs). Beginning at the 48 h forecasts, the differences in temperature and geopotential heights of the two experiments become larger (Figure 12). For the 48 h forecasts (1800 UTC on 2 October), the temperature of the hurricane center from CrIS (org) (Figure 12a) is colder than the temperature from CrIS (CCRs) (Figure 12e), which indicates that the warm-core center of CrIS (CCRs) is stronger than CrIS (org). For the 72 h forecasts (1800 UTC on 3 October), the longitude of the hurricane center from CrIS (org) (Figure 12b) is around 73° W; CrIS (CCRs) (Figure 12f) places it around 71°W. So the hurricane center of CrIS (org) is 2° to the west of CrIS (CCRs), moving it closer to the low pressure system over CONUS. For the 96 h forecasts (1800 UTC on 4 October), the hurricane center from CrIS (org) (Figure 12c) is moved toward the low-pressure system, and the two systems merged together at the 120 h forecasts (Figure 12d). For the 96 h forecasts of CrIS (CCRs) (Figure 12g), the hurricane center still moves east and has not merged with the low-pressure system over CONUS, which makes the track forecast closer to the observations. So based on the temperature and geopotential heights at 500 hPa, the hurricane core center is warmer and stronger from CrIS (CCRs) than that from CrIS (org), which makes the hurricane center merged with the low-pressure system over CONUS area and moves it to the east.

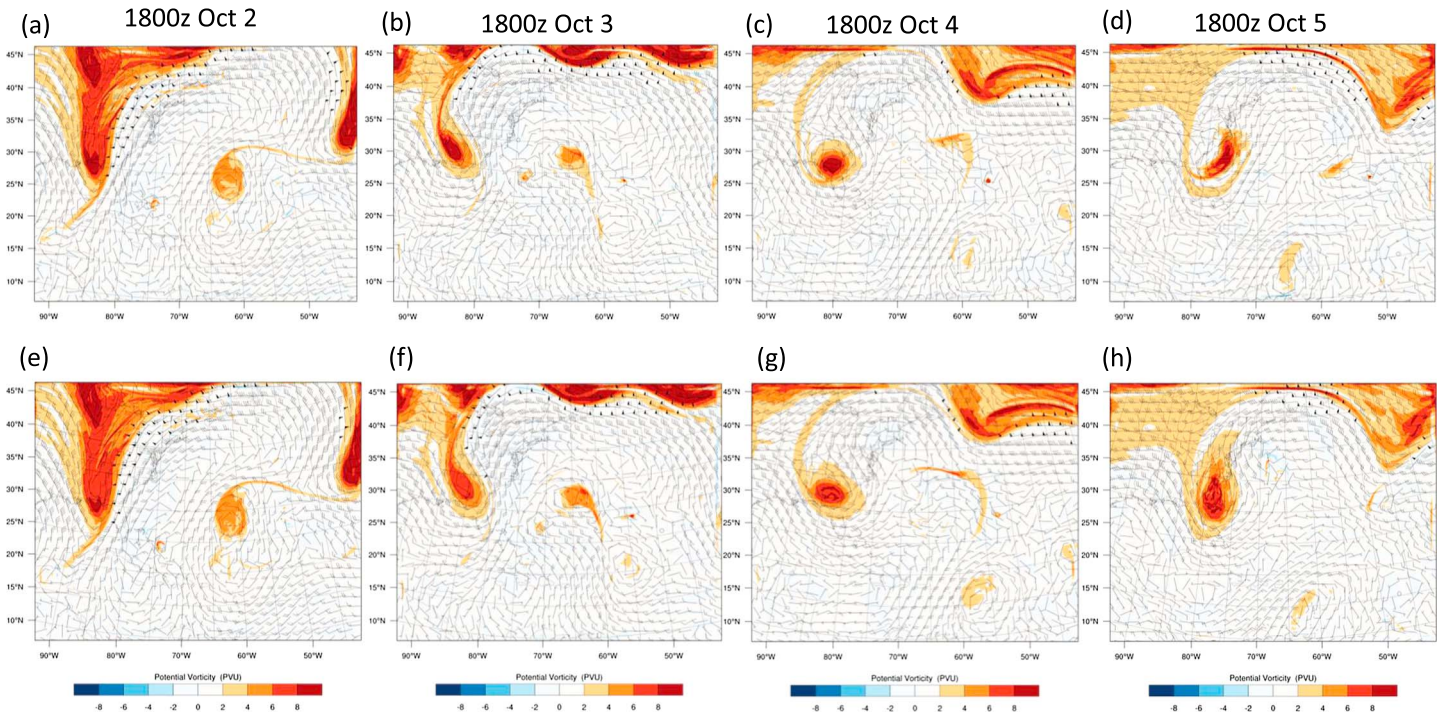

Figure 13. PV (shaded, unit: PVU) and wind vector (vector) at 200 hPa for 48 h, 72 h, 96 h, and 120 h forecast from (a–d) CrIS (org) and (e–h) CrIS (CCRs) from 1800 UTC on 30 September 2015.

Potential vorticity (PV) can be used to identify the intensity of cold weather in the upper troposphere. The PV and wind structure at 200 hPa are shown in Figure 13 for CrIS (org) and CrIS (CCRs) for the 120 h forecasts from 1800 UTC on 30 September. Based on the analysis of temperature and geopotential heights at 500 hPa, it is known that there is a cold low pressure over CONUS to the west of the hurricane center. The changes in PV trace the intensity of the cold low-pressure system. At 1800 UTC on 2 October, PV structures of CrIS (org) (Figure 13a) and CrIS (CCRs) (Figure 13e) are similar. At 1800 UTC on 3 October and 1800 UTC on 4 October, the PV over CONUS from CrIS (org) (Figure 13b) is warmer than from CrIS (CCRs) (Figure 13f), which indicates that the low-pressure system over CONUS is stronger from CrIS (org) than that from CrIS (CCRs). This also explained that the stronger low-pressure system over CONUS is the dominant system from CrIS (org), which makes the hurricane center move west and merge with the low-pressure system at the 120 h forecast. The relatively weaker low-pressure system over CONUS from CrIS (CCRs) is not the dominant system, so the hurricane center is still moving east to the Atlantic Ocean.

6. Discussion and Summary

The CC method has been adapted from MODIS/AIRS to retrieve VIIRS/CrIS CCRs by taking into account the spectral and geometry differences between MODIS/AIRS and VIIRS/CrIS observing systems. Compared with MODIS/AIRS for CCRs, the CrIS CCRs have a disadvantage, on the one hand, due to the lack of absorption bands in VIIRS, although two additional QC steps are applied; on the other hand, VIIRS has higher spatial resolution than MODIS and could provide a higher resolution cloud mask product than MODIS, and CrIS also has a better signal-to-noise ratio than AIRS. Therefore, the CrIS/VIIRS should produce reasonable CCRs for assimilation.

Validation of CrIS CCRs show reasonable accuracy and precision. The impact studies with Hurricane Joaquin (2015) and Hurricane Matthew (2016) indicate the assimilation of CrIS (CCRs) shows positive impacts on the analysis and forecast fields. The following conclusions can be drawn from this study.

1. The assimilation of CrIS CCRs can substantially increase the number of CrIS radiance observations assimilated for channels with weighting functions peaking at low levels, while a less substantial increase for channels with weighting functions peaking at high levels.

2. The data impacts of CrIS CCRs become larger with longer forecast times. The SD of both temperature and moisture fields from CrIS (CCRs) is the smallest among the three experiments especially beyond 72 h forecast. The assimilation of CrIS (CCRs) improves the hurricane track forecast compared with CrIS (org), but the impacts on the intensity forecasts are mixed or neutral.
3. Based on the two case studies of assimilating CrIS CCRs, additional information may be obtained from the CrIS CCRs to improve the analysis fields, which may further improve the forecast results.

Although the positive impact from CCRs becomes more obvious after 72 h forecasts, it is also noticeable in the short time forecasts when compared with dropwindsondes and the best track estimate. Since the observations assimilated are under clear and partially cloudy skies, which are mostly in the hurricane environment, it might take time to get the impacts from the environmental observations. Therefore, after 72 h, the positive impact could become more obvious. When CrIS (CCRs) are included, more data are assimilated from the environment, and the impacts of the assimilated data can become larger after 72 h forecast. The growth of positive impact is also consistent with the growth of forecast error.

The assimilation of CCRs is an alternative and effective way to use the thermodynamic information under partially cloudy regions. But the lack of observations from inside the hurricane center makes the intensity forecast hard to improve. So how to provide information from the hurricane core using IR observations still needs further studies. These two case studies provide a demonstration of the application of CrIS CCRs data. The advanced data assimilation system is used in operational centers, such as hybrid 3Dvar and 4Dvar systems, which are improvement compared to the 3Dvar system in this study. To generate the CrIS CCRs, it requires the CrIS level 1b, VIIRS level 1b, and VIIRS cloud-mask product, the latency of the cloud-clearing method should not pose significant barrier on operational applications, especially on regional applications. Therefore, more collaboration with operational centers for operational NWP models (i.e., GFS, HWRF and RAP) will be pursued in the future.

Acknowledgments
This work is supported by JPSS Risk Reduction and NOAA GOES-R high impact weather (HIW) and GYHY201406011. The view, opinions, and findings contained in this report are those of the authors and should not be construed as an official National Oceanic and Atmospheric Administration's or U.S. government's position, policy, or decision. We appreciate the CIMSS/SSEC sounding team for preparing the CrIS cloud-cleared data and the SSEC Data Center for providing the GOES-13 imager data. Thanks to JCSDA (Joint Center for Satellite Data Assimilation) for providing "S4" supercomputer (Supercomputer for Satellite Simulations and Data Assimilation) (Boukabara et al., 2016) physically located at SSEC of University of Wisconsin-Madison as the main computational resource for this research study.

References

Baker, N. (2012). Joint Polar Satellite System (JPSS) cloud top algorithm theoretical basis document (ATBD), 474–0041, 73 pp., NASA Goddard Space Flight Center, Greenbelt, MD.

Bauer, P., Auligné, T., Bell, W., Geer, A., Guidard, V., Heilliette, S., … Riishøjgaard, L.-P. (2011). Satellite cloud and precipitation assimilation at operational NWP centres. *Quarterly Journal of the Royal Meteorological Society*, *137*(661), 1934–1951. https://doi.org/10.1002/qj.905

Berg, R. (2016). Hurricane Joaquin (AL112015), National Hurricane Center tropical cyclone report, 1–36.

Boukabara, S., Zhu, T., Tolman, H. L., Lord, S., Goodman, S., Atlas, R., … Chen, T.-C. (2016). S4: An O2R/R2O infrastructure for optimizing satellite data utilization in NOAA numerical modeling systems: A step toward bridging the gap between research and operations. *Bulletin of the American Meteorological Society*, *97*(12), 2359–2378. https://doi.org/10.1175/BAMS-D-14-00188.1

Cardinali, C. (2009). Monitoring the observation impact on the short-range forecast. *Quarterly Journal of the Royal Meteorological Society*, *135*(638), 239–250. https://doi.org/10.1002/qj.366

Chen, Y., Han, Y., Van Delst, P., & Weng, F. (2010). On water vapor Jacobian in fast radiative transfer model. *Journal of Geophysical Research*, *115*, D12303. https://doi.org/10.1029/2009JD013379

Chen, Y., Han, Y., & Weng, F. (2012). Comparison of two transmittance algorithms in the community radiative transfer mode: Application to AVHRR. *Journal of Geophysical Research*, *117*, D06206. https://doi.org/10.1029/2011JD016656

Cucurull, L., Anthes, R. A., & Tsao, L.-L. (2014). Radio occultation observations as anchor observations in numerical weather prediction models and associated reduction of bias corrections in microwave and infrared satellite observations. *Journal of Atmospheric and Oceanic Technology*, *31*(1), 20–32. https://doi.org/10.1175/JTECH-D-13-00059.1

Eresmaa, R. (2014). Imager-assisted cloud detection for assimilation of Infrared Atmospheric Sounding Interferometer radiances. *Quarterly Journal of the Royal Meteorological Society*, *140*(684), 2342–2352. https://doi.org/10.1002/qj.2304

Garand, L., Buehner, M., Heilliette, S., Macpherson, S. R., & Beaulne, A. (2013). Satellite radiance assimilation impact in new Canadian ensemble-variational system, Proceedings of the 2013 EUMETSAT Meteorological Satellite Conference, 16–20 September, 2013, Vienna, Austria.

Geer, A. J., & Bauer, P. (2011). Observation errors in all-sky data assimilation. *Quarterly Journal of the Royal Meteorological Society*, *137*(661), 2024–2037. https://doi.org/10.1002/qj.830

Godin, R. (2014). Joint Polar Satellite System (JPSS) cloud effective particle size and cloud optical thickness algorithm theoretical basis document (ATBD), 474–0042, 148 pp., NASA Goddard Space Flight Center, Greenbelt, MD.

Han, H.-J., Li, J., Goldberg, M., Wang, P., Li, J., Li, Z., … Li, J. (2016). Microwave sounder cloud detection using a collocated high resolution imager and its impact on radiance assimilation in tropical cyclone forecasts. *Monthly Weather Review*, *144*, 3927–3959.

Han, Y., Van Delst, P., Liu, Q., Weng, F., Yan, B., Treadon, R., & Derber, J. (2006). JCSDA Community Radiative Transfer Model (CRTM) - Version 1, NOAA Tech Report 122.

Hong, S.-Y., & Lim, J.-O. J. (2006). The WRF single-moment 6-class microphysics scheme (WSM6). *Journal of the Korean Metrological Society*, *42*(2), 129–151.

Hutchison, K. D., Roskovensky, J. K., Jackson, J. M., Heidinger, A. K., Kopp, T. J., Pavolonis, M. J., & Frey, R. (2005). Automated cloud detection and typing of data collected by the Visible Infrared Imager Radiometer Suite (VIIRS). *International Journal of Remote Sensing*, *20*, 4681–4706.

Iacono, M. J., Delamere, J. S., Mlawer, E. J., Shephard, M. W., Clough, S. A., & Collins, W. D. (2008). Radiative forcing by long-lived greenhouse gases: Calculations with the AER radiative transfer models. *Journal of Geophysical Research*, *113*, D13103. https://doi.org/10.1029/2008JD009944

Joo, S., Eyre, J., & Marriott, R. (2013). The impact of MetOp and other satellite data within the Met Office global NWP system using an adjoint-based sensitivity method. *Monthly Weather Review*, *141*(10), 3331–3342. https://doi.org/10.1175/MWR-D-12-00232.1

Kain, J. S. (2004). The Kain-Fritsch convective parameterization: An update. *Journal of Applied Meteorology*, *43*(1), 170–181. https://doi.org/10.1175/1520-0450(2004)043%3C0170:TKCPAU%3E2.0.CO;2

Kelly, G., & Thepaut, J.-N. (2007). Evaluation of the impact of the space component of the Global Observation System through observing system experiments. ECMWF Newsletter, No. 113, ECMWF, Reading, United Kingdom, 16–28. Retrieved from http://www.ecmwf.int/publications/newsletters/pdf/113.pdf

Kleist, D. T., Parrish, D. F., Derber, J. C., Treadon, R., Wu, W.-S., & Lord, S. (2009). Introduction of the GSI into the NCEP global data assimilation system. *Weather Forecasting*, *24*(6), 1691–1705. https://doi.org/10.1175/2009WAF2222201.1

Le Marshall, J., Jung, J., Derber, J., Chahine, M., Treadon, R., Lord, S. J., … Tahara, Y. (2006). Improving global analysis and forecasting with AIRS. *Bulletin of the American Meteorological Society*, *87*(7), 891–894. https://doi.org/10.1175/BAMS-87-7-891

Le Marshall, J., Jung, J., Derber, J., Treadon, R., Lord, S., Goldberg, M., … Todling, R. (2005). AIRS hyperspectral data improves southern hemisphere forecasts. *Australian Meteorological Magazine*, *54*, 57–60.

Lee, T., Miller, S., Schueler, C., & Miller, S. (2006). NASA MODIS preview NPOESS VIIRS capabilities. *Weather Forecasting*, *21*(4), 649–655. https://doi.org/10.1175/WAF935.1

Li, J., Liu, C. Y., Huang, H.-L., Schmit, T. J., Menzel, W. P., & Gurka, J. (2005). Optimal cloud-clearing for AIRS radiances using MODIS. *IEEE Transactions on Geoscience and Remote Sensing*, *43*, 1266–1278.

Li, J., Menzel, W. P., Sun, F., Schmit, T. J., & Gurka, J. (2004). AIRS subpixel cloud characterization using MODIS cloud products. *Journal of Applied Meteorology*, *43*(8), 1083–1094. https://doi.org/10.1175/1520-0450(2004)043%3C1083:ASCCUM%3E2.0.CO;2

Li, J., Wang, P., Han, H., Li, J., & Zheng, J. (2016). On the assimilation of satellite sounder data in cloudy skies in the numerical weather prediction models. *Journal of Meteorology Research*, *30*(2), 169–182. https://doi.org/10.1007/s13351-016-5114-2

Li, J., Wang, P., Schmit, T. J., Li, J., Liu, C.-Y., & Li, Z. (2014). Handling clouds for hyperspectral infrared radiance assimilation, The 19th International TOVS Conference (ITSC-19), 26 March – 01 April 2014, Jeju Island, South Korea.

Lim, A. H. N., Jung, J. A., Huang, H.-L. A., Ackerman, S. A., & Otkin, J. A. (2014). Assimilation of clear sky atmospheric infrared sounder radiances in short-term regional forecasts using community models. *Journal of Applied Remote Sensing*, *8*(1), 083655. https://doi.org/10.1117/1.JRS.8.083655

Liu, H., Collard, A., & Derber, J. (2015). Variational cloud-clearing with CrIS data at NCEP, American Meteorological Society 2015, Phoenix, Arizona, January 5, 2015. Retrieved from http://www.jpss.noaa.gov/AMS–2015/Presentations /1–Variational–Cloudclearing–with–CrIS–data–at–NCEP.pdf

Liu, Z., Schwartz, C. S., Snyder, C., & Ha, S. Y. (2012). Impact of assimilating AMSU-A radiance on forecasts of 2008 Atlantic tropical cyclones initialized with a limited-area ensemble Kalman filter. *Monthly Weather Review*, *140*(12), 4017–4034. https://doi.org/10.1175/MWR-D-12-00083.1

McCarty, W., Jedlovec, G., & Miller, T. L. (2009). Impact of the assimilation of Atmospheric Infrared Sounder radiance measurements on short-term weather forecasts. *Journal of Geophysical Research*, *114*, 01/2009. https://doi.org/10.1029/2008JD011626

McNally, A. P., & Watts, P. D. (2003). A cloud detection algorithm for high-spectral-resolution infrared sounders. *Quarterly Journal of the Royal Meteorological Society*, *129*(595), 3411–3423. https://doi.org/10.1256/qj.02.208

Nagle, F. W. (1998). The association of disparate satellite observations, Proc. Second Symp. On Integrated Observing Systems, Phoenix, AZ *Amer. Meteor. Soc*., 49–52.

Nagle, F. W., & Holz, R. E. (2009). Computationally efficient methods of collocating satellite, aircraft, and ground observations. *Journal of Atmospheric and Oceanic Technology*, *26*(8), 1585–1595. https://doi.org/10.1175/2008JTECHA1189.1

Pangaud, T., Fourrie, N., Guidard, V., Dahoui, M., & Rabier, F. (2009). Assimilation of AIRS radiances affected by mid- to low-level clouds. *Monthly Weather Review*, *137*(12), 4276–4292. https://doi.org/10.1175/2009MWR3020.1

Pavelin, E. G., English, S. J., & Eyre, J. R. (2008). The assimilation of cloud-affected infrared satellite radiances for numerical weather prediction. *Quarterly Journal of the Royal Meteorological Society*, *134*(632), 737–749. https://doi.org/10.1002/qj.243

Pavolonis, M. J., & Heidinger, A. K. (2004). Daytime cloud overlap detection from AVHRR and VIIRS. *Journal of Applied Meteorology*, *43*(5), 762–778. https://doi.org/10.1175/2099.1

Smith, A., Atkinson, N., Bell, W., & Doherty, A. (2015). An initial assessment of observations from the Suomi-NPP satellite: Data from the Cross-track Infrared Sounder (CrIS). *Atmospheric Science Letters*, *16*(3), 260–266. https://doi.org/10.1002/asl2.551

Smith, W. L., Zhou, D. K., Huang, H.-L., Li, J., Liu, X., & Larar, A. M. (2004). Extraction of profile information from cloud contaminated radiances, *Proc. ECMWF Workshop on Assimilation of High Spectral Resolution Sounder in NWP*, Jun. 28-Jul. 1, 2004, pp. 145–154.

Susskind, J., Barnet, C., Blaisdell, J., Iredell, L., Keita, F., Kouvaris, L., … Chahine, M. (2006). Accuracy of geophysical parameters derived from Atmospheric Infrared Sounder/Advanced Microwave Sounding Unit as a function of fractional cloud cover. *Journal of Geophysical Research*, *111*, D09S17. https://doi.org/10.1029/2005JD006272

Wang, P., Li, J., Goldberg, M. D., Schmit, T. J., Lim, A. H. N., Li, Z., … Ackerman, S. A. (2015). Assimilation of thermodynamic information from advanced infrared sounders under partially cloudy skies for regional NWP. *Journal of Geophysical Research: Atmospheres*, *120*(11), 5469–5484. https://doi.org/10.1002/2014JD022976

Wang, P., Li, J., Li, J., Li, Z., Schmit, T. J., & Bai, W. (2014). Advanced infrared sounder subpixel cloud detection with imagers and its impact on radiance assimilation in NWP. *Geophysical Research Letters*, *41*, 1773–1780. https://doi.org/10.1002/2013GL059067

Wang, X., Parrish, D., Kleist, D., & Whitacker, J. (2013). GSI 3DVar-based ensemble-variational hybrid data assimilation for NCEP Global Forecast System: Single-resolution experiments. *Monthly Weather Review*, *140*, 4098–4117. https://doi.org/10.1175/MWR-D-12-00141.1

Wu, W.-S., Purser, R. J., & Parrish, D. F. (2002). Three- dimensional variational analysis with spatially inhomogeneous covariances. *Monthly Weather Review*, *130*(12), 2905–2916. https://doi.org/10.1175/1520-0493(2002)130%3C2905:TDVAWS%3E2.0.CO;2

Zhu, Y., Derber, J., Collard, A., Dee, D., Treadon, R., Gayno, G., & Jung, J. A. (2014). Enhanced radiance bias correction in the National Centers for Environmental Prediction's Gridpoint Statistical Interpolation data assimilation system. *Quarterly Journal of the Royal Meteorological Society*, *240*(682), 1479–1492.